JGR Solid Earth

RESEARCH ARTICLE
10.1029/2021JB023562

A Revised Adiabatic Temperature Profile for the Mantle

Tomoo Katsura[1]

[1]Bayerisches Geoinstitut, University of Bayreuth, Bayreuth, Germany

Key Points:

- The previous olivine-wadsleyite phase relations and P-V-T relations of mantle minerals are corrected using the pressure effect on electromotive force
- Comparing the 410-km discontinuity depth with the olivine-wadsleyite phase relations suggests 1839 (38) K at the discontinuity
- The adiabatic temperatures are 1646 (35) at 50-km depth and 2587 (60) K at 2,800-km depth

Supporting Information:

Supporting Information may be found in the online version of this article.

Correspondence to:

T. Katsura,
tomo.katsura@uni-bayreuth.de

Citation:

Katsura, T. (2022). A revised adiabatic temperature profile for the mantle. *Journal of Geophysical Research: Solid Earth*, *127*, e2021JB023562. https://doi.org/10.1029/2021JB023562

Received 4 NOV 2021
Accepted 31 JAN 2022

Author Contributions:

Conceptualization: Tomoo Katsura
Data curation: Tomoo Katsura
Formal analysis: Tomoo Katsura
Funding acquisition: Tomoo Katsura
Investigation: Tomoo Katsura
Methodology: Tomoo Katsura
Project Administration: Tomoo Katsura
Resources: Tomoo Katsura
Software: Tomoo Katsura
Validation: Tomoo Katsura
Visualization: Tomoo Katsura
Writing – original draft: Tomoo Katsura
Writing – review & editing: Tomoo Katsura

Abstract This study reevaluates the adiabatic temperature profile of the Earth's mantle. The global average temperature at the 410-km discontinuity is estimated to be 1839 (38) K by comparing the globally averaged depths of the 410-km discontinuity with the previously determined phase diagram of the olivine-wadsleyite transition in the system $(Mg,Fe)_2SiO_4$ at two temperatures. The temperature at the 410-km discontinuity is extrapolated to shallower and deeper regions using the adiabatic temperature gradient, which is estimated from the pressure-volume-temperature relations and heat capacities of the major mantle minerals, namely, olivine, wadselyite, ringwoodite, and bridgmanite. The experimental temperatures and pressures in the original studies used in these evaluations are recalculated using the recently proposed pressure correction on EMF of the $W_{97}Re_3$-$W_{75}Re_{25}$ thermocouple. The uncertainties are evaluated by the Monte Carlo simulation. The temperatures on the adiabatic temperature profile are found to be 1646 (35), 1994 (40), 1960 (40), and 2587 (60) K, respectively, at a 50-km depth, just above the 660-km discontinuity, just below the 660-km discontinuity, and at 2,800-km depth. The lower mantle temperatures in the current estimation are lower than those given by Katsura et al. (2010), https://doi.org/10.1016/j.pepi.2010.07.001. The 50-km depth temperature is slightly higher but generally agrees to that estimated from the melting of depleted peridotite.

Plain Language Summary This study estimates the temperature profile of the Earth's mantle by generally following the approach described in Katsura et al. (2010), https://doi.org/10.1016/j.pepi.2010.07.001. The estimation consists of two steps. First, the temperature at the 410-km seismic discontinuity (D410), at which the seismic wave velocities abruptly increase almost everywhere in the mantle, is evaluated. The D410 is usually attributed to the olivine-wadsleyite transition in peridotite. Comparing the globally averaged D410 depth with the phase diagram of the olivine-wadsleyite transition yields a D410 temperature of 1839 (38) K. Second, this temperature is extrapolated to shallower and deeper regions by assuming that the heat is mainly transferred by convection in the mantle. The temperature gradient in such cases is the product of the thermal expansion coefficient and the temperature divided by the density and the heat capacity. The thermal expansion coefficients of the major mantle mineral are obtained by recalculating our previous experimental data. We found that the temperatures at 50-km depth, the bottom of the mantle transition zone, the top of the lower mantle, and 2,800-km depth are found to be 1646 (35), 1994 (40), 1960 (40), and 2587 (60) K, respectively. The 50-km depth temperature is slightly higher but generally agrees to that estimated from the melting of depleted peridotite.

1. Introduction

The temperature is one of the essential parameters for modeling the dynamics of the Earth's interior. Therefore, estimating the temperature distribution in the mantle is a vital task in solid geophysics. However, we cannot directly measure temperatures in the Earth's deep interior. We can only estimate the temperature distribution by combining various information obtained by indirect methods. Since the thermal conductivity of silicate minerals is low, the temperature profile of the major part of the mantle should be close to adiabatic (Turcotte and Schubert, 2014). Although the temperature gradients in the lithosphere and D" layers should be steeper than the adiabat, and the temperature profile in the lower mantle might be deviated from the adiabat due to the high viscosity (Rudolph et al., 2015), the adiabatic temperature profile is considered a good approximation of the mantle geotherm. Therefore, it is helpful to obtain an adiabatic temperature profile of the mantle by fixing a temperature at one depth in the deep mantle for a better understanding of the mantle structure and dynamics.

For this reason, Katsura et al. (2010) estimated the adiabatic temperature distribution in the mantle. They first estimated the temperature at the 410-km seismic discontinuity (D410) by comparing the global average depth of the D410 with the olivine-wadsleyite transition pressure as a function of temperature (Katsura, Yamada,

et al., 2004). Then, they estimated the temperatures above and below the D410 using the formula of the adiabatic temperature gradient with depth as:

$$\left(\frac{dT}{dz}\right)_S = \frac{\alpha g T}{C_p} \quad (1)$$

where T is the temperature, z is the depth, α is the thermal expansivity of the constituent, g is the gravitational acceleration, and Cp is the isobaric heat capacity per weight of the constituent (Turcotte and Schubert, 2014). In their calculation, the mantle rocks were approximated by the Mg endmembers of olivine, wadsleyite, ringwoodite, and bridgmanite. The P-V-T relations of these minerals were determined using the multianvil in situ X-ray diffraction experiments by (Katsura, Yokoshi, et al., 2004; Katsura, Yokoshi, et al., 2009; Katsura, Shatskiy, Manthilake, Zhai, Fukui, et al., 2009; Katsura, Shatskiy, Manthilake, Zhai, Yamazaki, et al., 2009). The Cp for olivine, wadsleyite, and ringwoodite were taken from Saxena et al. (1993), and that for bridgmanite was calculated using the Debye model.

However, the adiabatic temperature profile by Katsura et al. (2010) has to be revised for the following reasons. First, the temperatures in (Katsura, Yamada, et al., 2004; Katsura, Yokoshi, et al., 2004; Katsura, Yokoshi, et al., 2009; Katsura, Shatskiy, Manthilake, Zhai, Fukui, et al., 2009; Katsura, Shatskiy, Manthilake, Zhai, Yamazaki, et al., 2009) were measured using $W_{97}Re_3$-$W_{75}Re_{25}$ thermocouples without any pressure correction. Nishihara et al. (2020) provided the pressure correction of the relations of the EMF (electromotive force) and temperature of the $W_{97}Re_3$-$W_{75}Re_{25}$ thermocouple. Therefore, the experimental data in (Katsura, Yamada, et al., 2004; Katsura, Yokoshi, et al., 2004; Katsura, Yokoshi, et al., 2009; Katsura, Shatskiy, Manthilake, Zhai, Fukui, et al., 2009; Katsura, Shatskiy, Manthilake, Zhai, Yamazaki, et al., 2009) should be recalculated using Nishihara et al. (2020) correction. Second, Tange et al. (2012) obtained more reliable *P-V-T* data of $MgSiO_3$ bridgmanite than Katsura, Yokoshi, et al. (2009). These data should be included in estimating the lower-mantle adiabatic profile. Third, the calculation program used in Katsura et al. (2010) contained errors leading to incorrect thermal expansivity evaluation, as shown later. Finally, two studies reported the global average depths of D410 for these 10 years (Huang et al., 2019; Waszek et al., 2021), which should be included in the temperature estimation at the D410.

This paper presents a revised average adiabatic temperature profile in the mantle by integrating the above-mentioned new data and using a newly made calculation program.

2. Methods

The current study estimates an adiabatic temperature profile in the mantle by the procedure very similar to Katsura et al. (2010). Namely, it first estimates the temperature at D410, then estimates the temperature gradient, finally calculates the temperature profile from the D410 temperature using the estimated temperature gradient. Details of the procedure are explained below.

2.1. Temperature at the 410-km Discontinuity

The current study first considers the most probable global average of the D410 depth. Chambers et al. (2005), Flanagan and Shearer (1998, 1999), Houser et al. (2008, 2016), and Huang et al. (2019) mapped the D410 depths globally and suggested the averaged depths of 418, 418, 409, 410, 411, and 416.8 km, respectively. Very recently, Waszek et al. (2021) reported the average D410 km depths of 410.0 and 414.4 km based on the SS and PP precursors. We use these eight depths for the estimation of the adiabatic temperature profile.

The current study employs the data given by Katsura, Yamada, et al. (2004) for the phase relations of the olivine-wadsleyite transition in $(Mg,Fe)_2SiO_4$. They synthesized coexisting olivine and wadsleyite in a multi-anvil press with temperatures measured by $W_{97}Re_3$-$W_{75}Re_{25}$ thermocouples and pressures estimated from MgO volumes by in situ X-ray diffraction using the *P-V-T* relations of MgO suggested by Matsui et al. (2000). Then, Katsura, Yamada, et al. (2004) measured the compositions of recovered olivine and wadsleyite grains using an electron probe microanalyzer (EPMA). In the current study, the temperatures in Katsura, Yamada, et al. (2004)

Table 1
Temperature, Pressure, and Phase Compositions of Coexisting Olivine and Wadsleyite

Run #	V/V_0^{MgO}	Temperature before correction (K)	Pressure before correction (GPa)	Temperature after correction (K)	Pressure after correction (GPa)	X_{Mg}^{Ol}	X_{Mg}^{Wd}
733	0.9738 (6)	1,900	14.24 (16)	1,964	14.64 (16)	0.951 (5)	0.923 (1)
734	0.9763 (3)	1,900	13.78 (11)	1,962	14.18 (11)	0.906 (5)	0.852 (7)
735	0.9788 (3)	1,900	13.33 (10)	1,961	13.71 (10)	0.862 (9)	0.792 (3)
763	0.9741 (5)	1,600	12.29 (13)	1,643	12.56 (13)	0.876 (6)	0.782 (6)
779	0.9785 (5)	1,600	13.33 (14)	1,645	13.62 (14)	0.979 (3)	0.947 (6)
780	0.9725 (6)	1,600	12.58 (15)	1,643	12.86 (15)	0.915 (6)	0.840 (4)

Note. The initial data are from Katsura, Yamada, et al. (2004).

are corrected using Nishihara et al. (2020) pressure correction of the EMF-temperature relations. The pressures in Katsura, Yamada, et al. (2004) are recalculated using these new temperatures and the two MgO equations of state (EOS) based on the third-order Birch-Murnaghan EOS and Vinet EOS by Tange et al. (2009).

The recalculated olivine-wadsleyite phase-relation data are fitted to Strixrude's (1997) equations to express the binary loops at the above two temperatures. One essential parameter in his equations is the Fe-Mg partition coefficients between olivine and wadsleyite, K_D^{Mg-Fe},

$$K_D^{Mg-Fe} = \frac{X^{Ol}_{Fe_2SiO_4} X^{Wd}_{Mg_2SiO_4}}{X^{Wd}_{Fe_2SiO_4} X^{Ol}_{Mg_2SiO_4}} \quad (2)$$

where X^j_i is the mole fraction of component i in phase j, and Π is the reduced pressure using the transition pressures of the endmembers of Mg_2SiO_4 and Fe_2SiO_4, $P_{Mg2SiO4}$ and $P_{Fe2SiO4}$, respectively as:

$$\Pi = \frac{P - P_{Fe_2SiO_4}}{P_{Mg_2SiO_4} - P_{Fe_2SiO_4}} \quad (3)$$

where P is the experimental pressure. The mole fraction of wadsleyite, f_{Wd}, is expressed as a function of Π with the parameter K_D^{Mg-Fe} as:

$$f_{wd}(\Pi) = \frac{x_{bulk}\left(1 - K_D^{Mg-Fe}\right) - K_D^{Mg-Fe\,\Pi} + K_D^{Mg-Fe}}{1 - K_D^{Mg-Fe\,1-\Pi} - K_D^{Mg-Fe\,\Pi} + K_D^{Mg-Fe}} \quad (4)$$

where x_{bulk} is the bulk mole fraction of the Fe_2SiO_4 component. Fitting the experimental data to Equations 2–4 yields K_D^{Mg-Fe}, $P_{Mg2SiO4,}$ and $P_{Fe2SiO4}$. Although Katsura et al. (2010), Katsura, Yamada, et al. (2004) assumed that the difference in the endmember transition pressures, $P_{Mg2SiO4}$–$P_{Fe2SiO4}$, is independent of the temperature, this assumption is not adopted in the current study.

Similar to Katsura et al. (2010), the current study assumes that the upper mantle comprises Hawaiian pyrolite, namely, $X_{Mg} = 0.89$ (X_{Mg} = Mg/(Mg + Fe)) (Green & Falloon, 1998). Stixrude (1997) suggested that the D410 depth corresponds to the pressure where the olivine-to-wadsleyite ratio is 1:2, namely, $f_{Wd} = 2/3$. The current study follows this idea to obtain the olivine-wadsleyite transition pressure in Hawaiian pyrolite ($P_{Ol\text{-}Wd,\ Py}$) as a function of temperature. Comparing the pressure corresponding to the D410 depth with $P_{Ol\text{-}Wd,\ Py}$ allows estimating the D410 temperature.

The uncertainties in the above estimations are evaluated using the Monte Carlo simulation by producing 1,000 replica sets of the phase relation data. This procedure produces the replica sets' data points, including pressure and compositions of olivine and wadsleyite, as:

$$x_i^j = x_i^0 + p \cdot \sigma_{x_i^0} \quad (5)$$

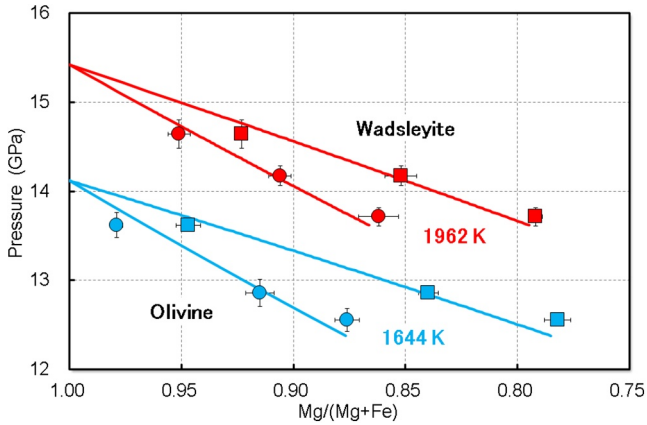

Figure 1. Binary phase relations of the olivine-wadsleyite transition in $(Mg,Fe)_2SiO_4$. The original data are from Katsura, Yamada, et al. (2004). The temperatures were recalculated using Nishihara et al. (2020) pressure correction of the EMF-temperature relations of $W_{97}Re_3$-$We_{75}Re_{25}$ thermocouple. The temperatures of 1600 and 1900 K in Katsura, Yamada, et al. (2004) became 1644 (blue) and 1962 (red) K. The circle and square symbols denote the compositions and pressures of coexisting olivine and wadsleyite, respectively.

where x^j_i is the ith data values in the jth replica data set, x^0_i and σx^0_i are the average and standard deviation of the ith datum in the original data set, and p is the normally distributed random number. Assuming the D410 depths of 409 and 411 km, the D410 temperatures are calculated for each replica set. The average and uncertainty of the D410 temperature are obtained from the mean value and standard deviation of the 1,000 replica sets at the two D410 depths.

2.2. Evaluation of the Parameters for the Adiabatic Temperature Gradient

The adiabatic temperature gradient with pressure is given as:

$$\left(\frac{dT}{dP}\right)_S = \frac{\alpha T}{\rho_c C_P} \tag{6}$$

where ρ_c is the density of the constituent (Turcotte and Schubert, 2014). Therefore, evaluating the adiabatic temperature gradient requires the thermal expansivity, density, and isobaric heat capacity of the constituents as a function of pressure and temperature.

Following Katsura et al. (2010), the current study approximates the mantle constituents by the Mg-endmembers of olivine, wadsleyite, ringwoodite, and bridgmanite at depth ranges of 50–410, 410–520, 520–660, and 660–2,800 km, respectively. Wolf et al. (2015) found that the adiabatic temperature gradients of $MgSiO_3$ and $(Mg_{0.83}Fe_{0.17})SiO_3$ bridgmanite are very similar, supporting the above approximation. On the other hand, although some studies suggested that the mantle transition zone contains weight percent levels of H_2O (Fei et al., 2017; Pearson et al., 2014), Houser (2016) predicted that the mantle transition zone is generally dry by combining the global analysis of long-period seismic data and the mineral physics data. Hence, we primarily assume that the Earth's mantle is essentially dry. In the latter part of this paper, we argue a possible effect of H_2O incorporation on estimating the adiabatic temperature profile.

The data sets for the density and thermal expansivity of olivine, wadsleyite, and ringwoodite are taken from (Katsura, Shatskiy, Manthilake, Zhai, Fukui, et al., 2009; Katsura, Shatskiy, Manthilake, Zhai, Yamazaki, et al., 2009; and Katsura, Yokoshi, et al., 2004, respectively. Those of bridgmanite are taken from Katsura, Yokoshi, et al., 2009 and Tange et al. (2012). The temperatures of these data sets are recalculated using Nishihara et al. (2020) pressure correction on the thermocouple EMF. The pressures are then recalculated based on these new temperatures using the two MgO EOS's given by Tange et al. (2009).

The P-V-T data set of each mineral is fitted to the Mie-Grüneisen-Debye EOS (Jackson & Rigden, 1996) with the third-order Birch-Murnaghan EOS (Katsura & Tange, 2019). At the standard temperature of $T_0 = 300$ K, the third-order Birch-Murnaghan EOS is expressed as:

$$P(V,T_0) = \frac{3}{2}K_{T_0}\left[\left(\frac{V_{P_0,T_0}}{V_{P,T_0}}\right)^{\frac{7}{3}} - \left(\frac{V_{P_0,T_0}}{V_{P,T_0}}\right)^{\frac{5}{3}}\right] \times \left\{1 - \frac{3}{4}\left(4 - K_{T_0}'\right)\left[\left(\frac{V_{P_0,T_0}}{V_{P,T_0}}\right)^{\frac{2}{3}} - 1\right]\right\} \tag{7}$$

where $P(V, T_0)$ is the pressure at volume V and the standard temperature of T_0, K_{T0} is the isothermal bulk modulus at the temperature of T_0, K_{T0}' is its pressure derivative, and $V_{P0,T0}$ and $V_{P,T0}$ are the volume at the standard pressure of $P_0 = 0$ and at the pressure of P, respectively, under the temperature condition of T_0. The Mie-Grüneisen-Debye EOS is:

$$P(V,T) = P(V,T_0) + \frac{\gamma}{V}\left[E_{\text{th}}(V_P,T) - E_{\text{th}}(V_P,T_0)\right] \tag{8}$$

where $P(V, T)$ is the pressure at the volume V and temperature T, γ is the Grüneisen parameter, and E_{th} is the thermal energy.

Table 2
Thermoelastic Parameters of the Major Mantle Minerals

Mineral	K_{T0} (GPa)	$K_{T_0}{}'$	θ (K)	γ_0	q
Olivine	127.4[a]	4.2 (4)	768[a]	1.00 (2)	2.4 (5)
Wadsleyite	169.2[b]	4.2 (2)	814[c]	1.23 (6)	1.5 (11)
Ringwoodite	188[d]	4.00 (4)	830[c]	1.28 (6)	2.4 (7)
Bridgmanite	256.7[e]	4.09 (4)	1030[f]	1.53 (3)	1.6 (4)

[a]Isaak et al. (1989). [b]Mao et al. (2008). [c]Watanabe et al. (1982). [d]converted from K_S given by Sinogeikin et al. (2003). [e]Tange et al. (2012). [f]Akaogi and Ito (1993).

The volume dependence of the Grüneisen parameter is expressed using the constant q as:

$$\gamma = \gamma_0 \left(\frac{V_{P,T}}{V_{P_0,T_0}} \right)^q \tag{9}$$

where γ_0 is the Grüneisen parameter at the standard pressure P_0 and temperature T_0. The thermal energy, E_{th}, is given by:

$$E_{\text{th}}(V,T) = \frac{9nRT}{(\theta/T)^3} \int_0^{\frac{\theta}{T}} \left(\frac{\xi^3}{e^\xi - 1} \right) \mathrm{d}\xi \tag{10}$$

where θ is the Debye temperature at the volume V, n is the number of atoms per formula unit, and R is the gas constant. The Debye temperature at the volume V is expressed as:

$$\theta = \theta_0 \ \exp\left[\frac{\gamma_0 - \gamma(V)}{q} \right] \tag{11}$$

where θ_0 is the Debye temperature at the standard volume V_0.

With the fixed values of K_{T0} and θ_0 given by literature (Akaogi & Ito, 1993; Higo et al., 2006; Isaak et al., 1989; Mao et al., 2008; Tange et al., 2012; Watanabe, 1982), the K_{T0}', γ_0, and q are fitted to minimize the sum of squared differences of the pressures based on each mineral's EOS, Pmineral, from those based on the MgO pressure marker using Tange et al. (2009) two EOS's, P_{MgO}. Namely, $\chi^2 = \Sigma(P_{\text{mineral}} - P_{\text{MgO}})^2$ is minimized.

The uncertainties of the fitting results of K_{T0}', γ_0, and q are evaluated using the Bootstrap method as follows. First, 1,000 bootstrap data sets are produced by randomly choosing data points from the original data set with allowing duplication. Then, uncertainties multiplied by the normally distributed random numbers are added to the individual data points using Equation 5. The three parameters of K_{T0}', γ_0, and q are obtained by fitting the individual bootstrap data sets to Equations 7–11. The averages and standard deviations of the three parameters are obtained from the mean values and standard deviations of the 1,000 bootstrap data sets. Note that the Bootstrap method is not adopted in modeling the phase relations because the number of the data points for the phase relations is too small for the bootstrap method (3 pairs of olivine and wadsleyite compositions at each temperature).

The density at given pressure and temperature is evaluated from the ambient density divided by the relative volumes given by Equations 7–10. The thermal expansivity is obtained from the differentiation of the relative volumes with respect to the temperature.

It is assumed that the isochoric heat capacity, C_V, of olivine is independent of the pressure because of the high temperatures. Therefore, the isobaric heat capacity at high pressure, C_P, can be obtained using the isobaric heat capacity of olivine at ambient pressure, $C_P{}^0$ as:

$$C_P = (1 + \alpha\gamma T) C_V = (1 + \alpha\gamma T) \frac{C_P^0}{1 + \alpha_0\gamma_0 T} = \frac{1 + \alpha\gamma T}{1 + \alpha_0\gamma_0 T} C_P^0 \tag{12}$$

where α and α_0 are the temperature-dependent thermal expansivities of olivine at high and ambient pressures, respectively. The isobaric heat capacity of olivine at ambient pressure is taken from Saxena et al. (1993), which was also adopted in Katsura et al. (2010).

The isobaric heat capacities of wadsleyite, ringwoodite, and bridgmanite are obtained by multiplying the Debye heat capacity by $1 + \alpha\gamma T$.

2.3. Evaluation of Adiabatic Temperature Profile in the Earth's Mantle

The adiabatic temperature gradient to the depth (z) in the mantle is written as:

$$\left(\frac{\mathrm{d}T}{\mathrm{d}z} \right)_S = \rho_{\text{m}} g \left(\frac{\mathrm{d}T}{\mathrm{d}P} \right)_S \tag{13}$$

Table 3
Adiabatic Temperature Profile in the Earth's Mantle

Depth (km)	*P* (GPa)	*T* (K)	d*T*/d*z* (K/km)
50	1.5	1646 (35)	0.54
70	2.1	1657 (35)	0.53
90	2.8	1667 (35)	0.51
100	3.1	1672 (36)	0.50
120	3.8	1682 (36)	0.48
140	4.4	1691 (36)	0.47
160	5.1	1700 (36)	0.46
180	5.8	1709 (37)	0.44
200	6.4	1718 (37)	0.43
220	7.1	1726 (37)	0.42
240	7.8	1735 (37)	0.41
260	8.5	1743 (38)	0.41
280	9.2	1751 (38)	0.40
300	9.9	1759 (38)	0.39
320	10.6	1766 (38)	0.38
340	11.2	1774 (38)	0.37
360	11.9	1781 (39)	0.36
380	12.6	1788 (39)	0.36
400	13.4	1796 (39)	0.37
410	13.7	1799 (39)	0.36
410	13.7	1860 (38)	0.36
420	14.1	1863 (38)	0.36
440	14.9	1871 (38)	0.36
460	15.6	1878 (38)	0.36
480	16.4	1885 (38)	0.35
500	17.1	1892 (39)	0.35
520	17.9	1899 (39)	0.35
520	17.9	1942 (39)	0.39
540	18.7	1950 (39)	0.38
560	19.5	1957 (39)	0.38
580	20.3	1965 (39)	0.37
600	21.0	1972 (39)	0.37
620	21.8	1980 (40)	0.36
640	22.6	1987 (40)	0.36
660	23.4	1994 (40)	0.37
660	23.4	1960 (40)	0.41
700	25.2	1976 (40)	0.40
800	29.6	2015 (41)	0.39
900	34.1	2053 (42)	0.37
1,000	38.6	2090 (43)	0.36
1,200	47.8	2158 (45)	0.33
1,400	57.3	2223 (47)	0.31
1,600	66.9	2283 (48)	0.29

where ρ_m and g are the density and gravity acceleration at a certain depth of the Earth's mantle given by PREM (Dziewonski & Anderson, 1981). Note that the ρ_m in this equation is different from ρ_c in Equation 6. The former is the density of the Earth's mantle, which consists of Fe-bearing peridotite. On the other hand, the latter is that of the Fe-free endmembers of the major mantle minerals. Katsura et al. (2010) did not consider this difference and simply obtained the adiabatic temperature gradient to the depth using Equation 1, which is the major error source of Katsura et al. (2010).

Using Equation 13, the temperatures at depths are obtained by 10-km increments and decrements from the D410 depth to deeper and shallower depths, respectively. It is well-known that the latent heat associated with the phase transition of olivine to wadsleyite, wadsleyite to ringwoodite, and ringwoodite to bridgmanite + ferropericlase abruptly changes the temperature profile (Ito & Katsura, 1989; Katsura et al., 2010). Following Katsura et al. (2010), the current study assumes the temperature change of +60, +43, and −34 K by these transitions. Since the D410 is taken as the depth where the olivine and wadsleyite have a volume ratio of 1:2 (Stixrude, 1997), the temperature changes of +20 and −40 K are delivered above and below the D410, as Katsura et al. (2010) did. The wadsleyite to ringwoodite and ringwoodite to bridgmanite + ferropericlase transitions are assumed to occur at fixed depths of 520 and 660 km, respectively.

3. Results and Discussion

3.1. Olivine-Wadsleyite Transition in $(Mg,Fe)_2SiO_4$

Table 1 presents the recalculated pressures and temperatures with the olivine and wadsleyite compositions from Katsura, Yamada, et al. (2004) experiments. Figure 1 shows the recalculated phase relations of the olivine-wadsleyite transitions in $(Mg,Fe)_2SiO_4$. The Nishihara et al. (2020) pressure correction of thermocouple EMF has increased from 1600 and 1900 K to 1644 and 1962 K, respectively. This correction has accordingly increased the pressures by 0.22 and 0.32 GPa at these temperatures, respectively. The fitting yields $K_D^{Mg-Fe} = 0.517 \pm 0.036$, $P_{Mg2SiO4} = 14.11 \pm 0.14$ GPa, and $P_{Fe2SiO4} = 3.6 \pm 1.1$ GPa at 1962 K and $K_D^{Mg-Fe} = 0.599 \pm 0.035$, $P_{Mg2SiO4} = 15.42 \pm 0.18$ GPa, and $P_{Fe2SiO4} = 4.6 \pm 1.1$ GPa at 1962 K. Consequently, the Clapeyron slopes of the Mg and Fe endmember transitions are 4.1 ± 0.5 and 3.4 ± 3.6 MPa/K, respectively. The uncertainties of $P_{Fe2SiO4}$ estimation (1.0 and 1.0 GPa) are 6–8 times larger than those of $P_{Mg2SiO4}$ (0.13 and 0.17 GPa). This is because Katsura, Yamada, et al. (2004) conducted the experiments with the bulk compositions around $X_{Mg} = 0.9$. The estimated $P_{Mg2SiO4}$ and $P_{Fe2SiO4}$ are anticorrelated, as expected (Figure S1 in Supporting Information S1).

Yagi et al. (1987) determined the fayalite-ahrensite transition in Fe_2SiO_4 using in situ X-ray diffraction with a multi-anvil press. Their data suggested $P_{Fe2SiO4}$'s of 7.0 ± 0.1 and 6.2 ± 0.1 GPa at 1644 and 1962 K, respectively, which are significantly higher than those estimated in the current study. Hence, the binary loop should have an old-crescent shape. However, these curvatures should be insignificant for the current study because the compositional range of Katsura, Yamada, et al. (2004) already covers the mantle composition ($X_{Mg} = 0.89$ (Green & Falloon, 1998; Figure 1).

Table 3
Continued

Depth (km)	P (GPa)	T (K)	dT/dz (K/km)
1,800	76.8	2340 (50)	0.28
2,000	86.9	2394 (52)	0.26
2,200	97.3	2445 (54)	0.25
2,400	108.0	2494 (56)	0.24
2,600	119.0	2541 (58)	0.23
2,800	130.4	2587 (60)	0.23

3.2. Temperature at the 410-km Discontinuity

The olivine-wadsleyite transition pressures in Hawaiian pyrolite, $P_{\text{Ol-Wd, Py}}$, are found to be 13.09 ± 0.07 and 14.34 ± 0.08 GPa at temperatures of 1644 and 1962 K, respectively. The smaller uncertainties in $P_{\text{Ol-Wd, Py}}$ than P_{Mg2SiO4} are because Katsura, Yamada, et al. (2004) conducted the experiments with the bulk compositions around $X_{\text{Mg}} = 0.9$ and not at $X_{\text{Mg}} = 1.0$ or equivalently because the P_{Mg2SiO4} and P_{Fe2SiO4} are anticorrelated.

The temperature dependence of $P_{\text{Ol-Wd, Py}}$ is $dP_{\text{Ol-Wd, Py}}/dT = 3.9 \pm 0.3$ MPa/K. This temperature dependence is significant because the temperature increase by 100 K causes the olivine-wadsleyite transition pressure to increase by 9.8 ± 0.7 km. In other words, 1-km variation of D410 depths should correspond to a temperature variation of 10.2 ± 0.7 K. Comparing $P_{\text{Ol-Wd, Py}}$ with the pressures of the D410 depths suggests the temperature at D410 to be 1839 ± 38 K. This temperature is identical to that estimated by Katsura et al. (2010), 1830 ± 48 K within the errors. This agreement has been made by the cancellation of the D410 depths, the used MgO equation of state, and the thermocouple correction. Katsura et al. (2010) adopted 409 km as the D410 depth, whereas the current study uses 8 reported depths, whose average depth is 413 ± 4 km. This increase in depth has raised the temperature by 40 K. Katsura et al. (2010) used Matsui et al. (2000) *P-V-T* relations of MgO in addition to Tange et al. (2009) EOS's. Matsui et al. (2000) data provided 80 and 40 K lower temperatures than Tange et al. (2009) Vinet- and Birch-Murnaghan EOSs. The thermocouple correction raises not only temperatures but also pressures of the experimental data points. The ratio of the pressure increase to the temperature increase is equal to the thermal pressure of MgO, which is 6.4 MPa/K at around 13 GPa and 1900–1600 K based on Tange et al. (2009). On the other hand, the temperature dependence of $P_{\text{Ol-Wd, Py}}$ is smaller, i.e., 3.9 ± 0.3 MPa/K. As a result, the required temperature for the olivine-wadsleyite transition becomes 50 K lower by the thermocouple correction. Also, note that the uncertainty in the temperature estimation is smaller in the current study than in Katsura et al. (2010). This smaller uncertainty is because Katsura et al. (2010) did not consider the anticorrelation of P_{Mg2SiO4} and P_{Fe2SiO4}.

3.3. *P-V-T* Relations of Major Mantle Minerals

Tables S1–S4 in Supporting Information S1 show the recalculated *P-V-T* data of the four minerals. Table 2 presents the optimized values together with the assumed parameters. Figures S2–S5 in Supporting Information S1 show the comparisons of pressures obtained using the Tange et al. (2009) MgO EOSs and the EOS of each mineral in the current study.

The obtained K' of the four minerals are identical within the uncertainties (Table 2). A higher-pressure mineral has a larger γ_0. This is reasonable because, according to the definition, γ_0 is the rate of the pressure increase to the thermal energy increase at constant volume and ambient pressure. Since the thermal expansivity of minerals vastly increases with decreasing pressure below their stability fields, the pressure increase rate caused by the energy increase should be more significant at ambient pressure in higher-pressure minerals.

However, the relation between the stability field and q among different minerals is unclear due to the significant uncertainties. Although ringwoodite apparently has a larger q than wadsleyite (2.4 ± 0.7 and 1.5 ± 1.1), this difference is within the uncertainties. As expected, the γ_0 and q are strongly correlated, especially for wadsleyite and ringwoodite due to their narrow experimental pressure ranges (Figure S6 in Supporting Information S1). Consequently, the uncertainty in q has a relatively small effect on the estimations of density and thermal expansivity.

3.4. Adiabatic Temperature Profile in the Earth's Mantle

Table 3 shows the adiabatic temperature profile in the mantle at depths from 50 to 2,800 km obtained in the current study. Although the temperature profile in the real mantle should not be adiabatic in the lower-most region due to the thermal boundary layer, the present profile is constructed by ignoring the presence of the thermal boundary layer. Table S5 in Supporting Information S1 shows various thermoelastic parameters at depths from 50 to 2,800 km with a 10-km step. Among the shown parameters in Table S5 in Supporting Information S1,

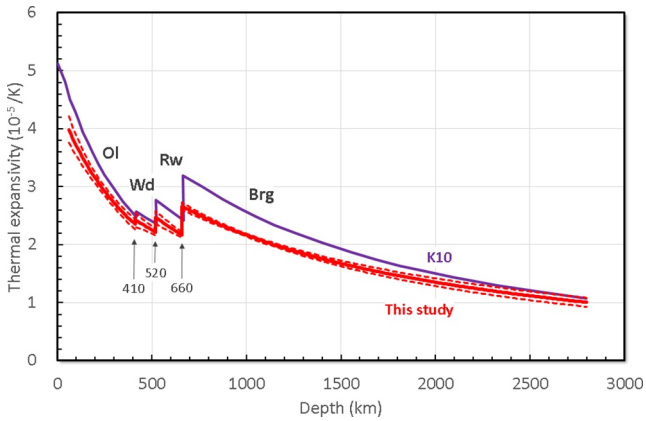

Figure 2. Thermal expansivity in the mantle. Red: The current study and violet: Katsura et al. (2010). The solid and dashed curves show the most probable and 68% confidence intervals, respectively.

the density, gravitational acceleration, and pressure are taken from PREM (Dziewonski & Anderson, 1981). The other parameters are obtained through the procedure described above. The thermal expansivity, adiabatic temperature gradient, and adiabatic temperature profile are plotted in Figures 2–4.

As Katsura et al. (2010) argued, the thermal expansivity continuously decreases with increasing depth due to the negative temperature dependence when no phase transition occurs, whereas the phase transitions increase the thermal expansivity (Figure 2). In the olivine stability field, the thermal expansivity decreases from $(4.1 \pm 0.2) \times 10^{-15}$ to $(2.4 \pm 0.1) \times 10^{-15}$ K^{-1} down to 410-km depth. In the wadsleyite and ringwoodite stability fields, it decreases from $(2.4 \pm 0.1) \times 10^{-15}$ to $(2.2 \pm 0.5) \times 10^{-15}$ and from $(2.5 \pm 0.1) \times 10^{-15}$ to $(2.2 \pm 0.5) \times 10^{-15}$ K^{-1}, respectively, at 410–520 and 520–660 km depths. In the bridgmanite stability field, it decreases from $(2.7 \pm 0.5) \times 10^{-15}$ to $(1.1 \pm 0.1) \times 10^{-15}$ K^{-1} to 2800-km depth. These values are about 10% smaller than those of Katsura et al. (2010). Since the data sources are very similar between the current study and Katsura et al. (2010), could have miscalculated the thermal expansivity.

Since the other parameters for the adiabatic temperature gradient given by Equation 13 other than the thermal expansivity do not vary significantly, the adiabatic temperature gradient varies similarly to the thermal expansivity (Figures 2 and 3). The adiabatic temperature gradient continuously decreases with depth without a phase transition, whereas it increases when a phase transition occurs. In the olivine stability field, the adiabatic gradient decreases from (0.54 ± 0.03) to (0.36 ± 0.02) K km^{-1} down to 410-km depth. In the wadsleyite and ringwoodite stability fields, it decreases from 0.36 ± 0.02–0.35 ± 0.01 and from 0.39 ± 0.02–0.37 ± 0.01 K km^{-1}, respectively, at 410–520 and 520–660 km depths. In the bridgmanite stability field, it decreases from 0.41 ± 0.01–0.23 ± 0.02 K km^{-1} to 2800-km depth. As expected, the current adiabatic gradient is smaller than Katsura et al. (2010), similar to the thermal expansivity. On the other hand, the adiabatic gradient in the lower mantle from the current study agrees very well to those estimated by Wolf et al. (2015), which has gradients of 0.35–0.39 K/km at the top of the lower mantle and decrease to 0.25–0.27 K/km at 2,300-km depth. Turcotte and Schubert (2014) suggested an adiabatic temperature gradient of 0.3 K km^{-1} in the mantle. This value may be a good approximation in the regions from the bottom of the upper mantle to the mid-mantle, but it may be underestimated for the uppermost mantle and overestimated for the deeper regions of the lower mantle.

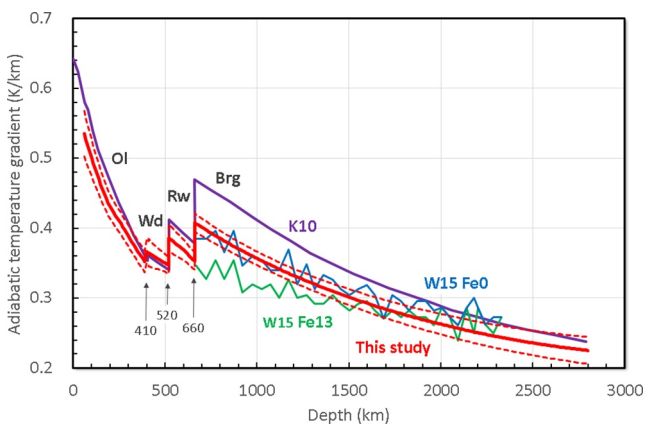

Figure 3. Adiabatic temperature gradients in the mantle. Red: The current study; violet: Katsura et al. (2010); blue: $MgSiO_3$ bridgmanite lower mantle by Wolf et al. (2015); green: $Mg_{0.87}Fe_{0.13}SiO_3$ bridgmanite lower mantle by Wolf et al. (2015). The solid and dashed curves show the most probable and 68% confidence intervals, respectively.

According to the above argument, the temperatures are 1799 ± 39 and 1860 ± 38 K, respectively, just above and below the D410, 1899 ± 39 and 1942 ± 39 K, respectively, just above and below 520-km depth, and 1994 ± 40 and 1960 ± 40 K, respectively, just above and below 660-km depth (Table 2 and Figure 4). The temperature at 50-km depth is 1646 ± 35 K, whereas that at 2800-km depth is 2587 ± 60 K. An extrapolation of the temperature at 50-km depth to the surface using the temperature gradient at 50-km depth (0.54 K km^{-1}) yields the mantle potential temperature of 1619 K (1350°C). The upper mantle temperatures essentially have no change from Katsura et al. (2010). On the other hand, the lower mantle temperatures are becoming lower with depth compared to Katsura et al. (2010). The 2800-km depth temperature in the current study is about 80 K lower than that of Katsura et al. (2010). The reason for this discrepancy is that Katsura et al. (2010) miscalculated the thermal expansion coefficients of bridgmanite at shallower depths (Figure 2), leading to overestimation of the adiabatic temperature gradient in the lower mantle. Wolf et al. (2015) reported an adiabatic temperature profile in the lower mantle down to 2400-km depth. He suggested a temperature of 2390 K at 2400-km depth, which is 100 K lower than the current study (2490 K). This is because Wolf et al. (2015) arbitrarily assumed the temperature at 670-km depth of 1873 K, which is ca.

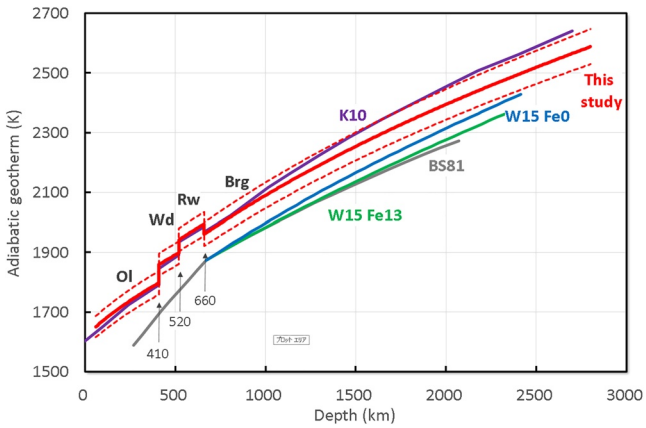

Figure 4. Adiabatic temperature profiles in the mantle. Red: The current study; violet: Katsura et al. (2010); blue: $MgSiO_3$ bridgmanite lower mantle by Wolf et al. (2015); green: $Mg_{0.87}Fe_{0.13}SiO_3$ bridgmanite lower mantle by Wolf et al. (2015); gray: Brown and Shankland (1981). The solid and dashed curves show the most probably and 68% confidence intervals, respectively.

90 K higher than the present estimation (1960 K) (Figure 4). Brown and Shankland (1981) estimated the adiabatic temperature profile and reported 140 K lower temperature at 2070 km depth (2410 K) than the current study (Figure 4), which is also caused by the assumption of 1873 K at the top of the lower mantle in Brown and Shankland (1981).

Sarafian et al. (2017) determined the solidus temperature of mantle peridotite with 140 wt. ppm of H_2O at a pressure of 1.5 GPa, corresponding to 50 km depth. Their solidus temperature was 1590 ± 10 K, which is slightly lower than that of the present profile, 1646 ± 35 K. The peridotite melting may start at slightly deeper regions than 50-km depth, and the melt finally may separate from the source rocks at around 50 km depth beneath mid-oceanic ridges.

3.5. Uncertainties Due to Possible Compositional Effects

Finally, we argue the chemistry effects on estimating the temperature profile, first the uniformity of constituting rocks, and second the H_2O incorporation.

Xu et al. (2008) examined a possibility that the mantle comprises a mechanical mixture of harzburgite and basalt (MM) rather than an equilibrium assemblage of pyrolitic composition (EA). If the Hawaiian pyrolite (Green & Falloon, 1998) and dunite/harzburgite (Afonso et al., 2008) represent pyrolite and harzburgite compositions, their X_{Mg} are 0.89 and 0.93, respectively. Since the olivine-wadsleyite transition should not occur in the basaltic part but only in the harzburgite part in the MM mantle, the harzburgite composition controls the transition pressure with temperature. Due to the higher X_{Mg}, the olivine-wadsleyite transition pressures in harzburgite ($P_{Ol\text{-}Wd,\ Hz}$) are higher than those in Hawaiian pyrolite: 13.47 and 14.72 GPa at 1644 and 1962 K, respectively. As a result, the D410 occurs at 10 km deeper depths at the same temperature. Consequently, the estimated D410 temperature is decreased by 100 K. The temperature profile with this D410 temperature is presented in Table S6 in Supporting Information S1 and depicted in Figure 5. In this profile, the temperature at a 50-km depth is 1559 ± 35 K. This temperature is slightly lower than the temperature required for the MORB magmatism given by Sarafian et al. (2017) (1590 ± 10 K), although the difference is still within the errors.

Pearson et al. (2014) discovered a diamond inclusion of ringwoodite with 1.4 wt% of H_2O. Therefore, the mantle transition is at least locally wet. Here, we examine the effect of 1.4 wt% H_2O incorporation on the temperature profile. Chen et al. (2002) demonstrated that the binary loop of the olivine-wadsleyite loop shifts toward lower pressure. Hence, the H_2O incorporation should raise the D410, and the estimated temperature at the D410 should become higher. Inoue et al. (2010) studied the effect of 1 wt% bulk H_2O on the olivine-wadsleyite transition pressures at a temperature of 1673 K. Their diagram implies that the 1 wt% H_2O incorporation lowers the transition pressure by 0.2 GPa at X_{Mg} = 0.9. Hence, 1.4 wt% of H_2O raises the D410 by 7 km (0.3 GPa), increasing the estimated temperature by 70 K. Inoue et al. (2004) measured the thermal expansivity of hydrous wadsleyite and ringwoodite with 2.4 and 2.6 wt% of H_2O at temperatures of 290–620 K and compared them with their dry counterparts. Their results implied that a 1.4% of H_2O incorporation should decrease the thermal expansivity of wadsleyite and ringwoodite from 3.4×10^{-15} to 3.2×10^{-15} K and from 3.1×10^{-15} to 2.9×10^{-15} K. From these evaluations, we calculate an adiabatic temperature profile as presented in Table S7 in Supporting Information S1 and depicted in Figure 5. Since the solidus of H_2O-saturated mantle peridotite is located at 1300 K at pressures of 5–11 GPa (Kawamoto and Holloway, 1997), however, this temperature profile is too high for the mantle to be solid. Hence, it is concluded that the mantle is globally dry.

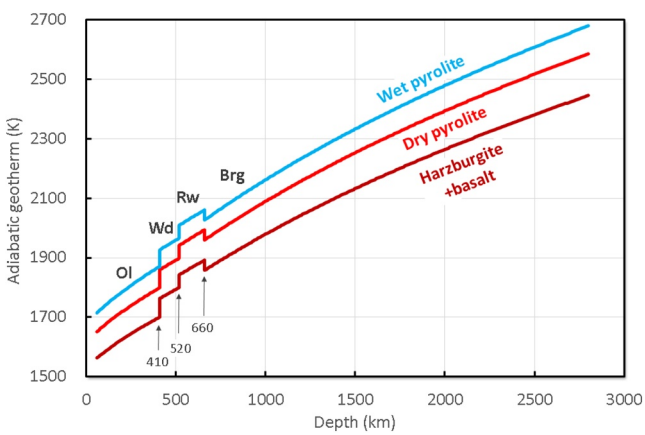

Figure 5. Adiabatic temperature profiles of dry pyrolite (red), harzburgite + basalt mixture (dark red), and wet pyrolite (cyan).

Data Availability Statement

The P-V-T data used in this study after the EMF correction using Nishihara et al. (2020) and the pressure calculation using Tange et al. (2009) are given at https://doi.org/10.5281/zenodo.5644426. The Matlab scripts to fit the P-V-T data to the equations of state, the temperature at the 410-km discontinuity, and calculate the adiabatic temperature profile are given at https://doi.org/10.5281/zenodo.5903286.

Acknowledgments
The author thanks H. Fei, A. Chakraborti, F. Wang, L. Wang, and D. Bondar for reading and commenting on the manuscript. The current study is supported by the European Research Council (ERC) under Horizon 2020 research and innovation program (grant agreement No. 787527). There is no conflict of interest. Open access funding enabled and organized by Projekt DEAL.

References

Afonso, J. C., Fernandez, M., Ranalli, G., Griffin, W. L., & Connolly, J. A. D. (2008). Integrated geophysical-petrological modeling of the lithosphere and sublithospheric upper mantle: Methodology and applications. *Geochemistry, Geophysics, Geosystems*, *9*, 36. https://doi.org/10.1029/2007gc001834

Akaogi, M., & Ito, E. (1993). Heat capacity of $MgSiO_3$ perovskite. *Geophysical Research Letters*, *20*(2), 105–108. https://doi.org/10.1029/92GL02655

Brown, J. M., & Shankland, T. J. (1981). Thermodynamic parameters in the Earth as determined from seismic profiles. *Geophysical Journal of the Royal Astronomical Society*, *66*(3), 579–596. https://doi.org/10.1111/j.1365-246X.1981.tb04891.x

Chambers, K., Woodhouse, J. H., & Deuss, A. (2005). Topography of the 410-km discontinuity from PP and SS precursors. *Earth and Planetary Science Letters*, *235*(3–4), 610–622. https://doi.org/10.1016/j.epsl.2005.05.014

Chen, J. H., Inoue, T., Yurimoto, H., & Weidner, D. J. (2002). Effect of water on olivine-wadsleyite phase boundary in the $(Mg, Fe)_2SiO_4$ system. *Geophysical Research Letters*, *29*, 1875. https://doi.org/10.1029/2001gl014429

Dziewonski, A. M., & Anderson, D. L. (1981). Preliminary reference earth model. *Physics of the Earth and Planetary Interiors*, *25*(4), 297–356. https://doi.org/10.1016/0031-9201(81)90046-7

Fei, H., Yamazaki, D., Sakurai, M., Miyajima, N., Ohfuji, H., Katsura, T., & Yamamoto, T. (2017). A nearly water-saturated mantle transition zone inferred from mineral viscosity. *Science Advances*, *3*(6), e1603024. https://doi.org/10.1126/sciadv.1603024

Flanagan, M. P., & Shearer, P. M. (1998). Global mapping of topography on transition zone velocity discontinuities by stacking SS precursors. *Journal of Geophysical Research: Solid Earth*, *103*(B2), 2673–2692. https://doi.org/10.1029/97JB03212

Flanagan, M. P., & Shearer, P. M. (1999). A map of topography on the 410-km discontinuity from PP precursors. *Geophysical Research Letters*, *26*(5), 549–552. https://doi.org/10.1029/1999GL900036

Green, D. H., & Falloon, T. J. (1998). Pyrolite: A Ringwood Concept and its current expression. In I. Jackson (Ed.), *The Earth's mantle* (pp. 311–378). Cambridge University Press. https://doi.org/10.1017/CBO9780511573101.010

Higo, Y., Inoue, T., Li, B. S., Irifune, T., & Liebermann, R. C. (2006). The effect of iron on the elastic properties of ringwoodite at high pressure. *Physics of the Earth and Planetary Interiors*, *159*(3–4), 276–285. https://doi.org/10.1016/j.pepi.2006.08.004

Houser, C. (2016). Global seismic data reveal little water in the mantle transition zone. *Earth and Planetary Science Letters*, *448*, 94–101. https://doi.org/10.1016/j.epsl.2016.04.018

Houser, C., Masters, G., Flanagan, M., & Shearer, P. (2008). Determination and analysis of long-wavelength transition zone structure using SS precursors. *Geophysical Journal International*, *174*(1), 178–194. https://doi.org/10.1111/j.1365-246X.2008.03719.x

Huang, Q., Schmerr, N., Waszek, L., & Beghein, C. (2019). Constraints on seismic anisotropy in the mantle transition zone from long-period SS precursors. *Journal of Geophysical Research: Solid Earth*, *124*, 6779–6800. https://doi.org/10.1029/2019JB017307

Inoue, T., Tanimoto, Y., Irifune, T., Suzuki, T., Fukui, H., & Ohtaka, O. (2004). Thermal expansion of wadsleyite, ringwoodite, hydrous wadsleyite and hydrous ringwoodite. *Physics of the Earth and Planetary Interiors*, *143–44*, 279–290. https://doi.org/10.1016/j.pepi.2003.07.021

Inoue, T., Ueda, T., Tanimoto, Y., Yamada, A., & Irifune, T. (2010). The effect of water on the high-pressure phase boundaries in the system Mg_2SiO_4-Fe_2SiO_4. *Journal of Physics: Conference Series*, *215*, 01210. https://doi.org/10.1088/1742-6596/215/1/012101

Isaak, D. G., Anderson, O. L., Goto, T., & Suzuki, I. (1989). Elasticity of single-crystal forsterite measured to 1700 K. *Journal of Geophysical Research: Solid Earth*, *94*, 5895–5906. https://doi.org/10.1029/jb094ib05p05895

Ito, E., & Katsura, T. (1989). A temperature profile of the mantle transition zone. *Geophysical Research Letters*, *16*(5), 425–428. https://doi.org/10.1029/GL016i005p00425

Jackson, I., & Rigden, S. M. (1996). Analysis of P-V-T data: Constraints on the thermoelastic properties of high-pressure minerals. *Physics of the Earth and Planetary Interiors*, *96*(2–3), 85–112. https://doi.org/10.1016/0031-9201(96)03143-3

Katsura, T., Shatskiy, A., Manthilake, M., Zhai, S., Yamazaki, D., Matsuzaki, T., et al. (2009). P-V-T relations of wadsleyite determined by in situ X-ray diffraction in a large-volume high-pressure apparatus. *Geophysical Research Letters*, *36*(11), L11307. https://doi.org/10.1029/2009GL038107

Katsura, T., Shatskiy, A., Manthilake, M., Zhai, S., Fukui, H., Yamazaki, D., et al. (2009). Thermal expansion of forsterite at high pressures determined by in situ X-ray diffraction: The adiabatic geotherm in the upper mantle. *Physics of the Earth and Planetary Interiors*, *174*(1–4), 86–92. https://doi.org/10.1016/j.pepi.2008.08.002

Katsura, T., & Tange, Y. (2019). A simple derivation of the Birch-Murnaghan equations of state (EOSs) and comparison with EOSs derived from other definitions of finite strain. *Minerals*, *9*(12), 745. https://doi.org/10.3390/min9120745

Katsura, T., Yamada, H., Kubo, A., Shinmei, T., Nishikawa, O., Yoshino, T., et al. (2004). Olivine–wadsleyite transition in the system $(Mg,Fe)_2SiO_4$. *Journal of Geophysical Research: Solid Earth*, *109*(2), B02209. https://doi.org/10.1029/2003JB002438

Katsura, T., Yokoshi, S., Kawabe, K., Shatskiy, A., Manthilake, M., Zhai, S., et al. (2009). P-V-T relations of $MgSiO_3$ perovskite determined by in situ X-ray diffraction using a large-volume high-pressure apparatus. *Geophysical Research Letters*, *36*(1), L01305. https://doi.org/10.1029/2009GL039318

Katsura, T., Yokoshi, S., Song, M., Kawabe, K., Tsujimura, T., Kubo, A., et al. (2004). Thermal expansion of Mg_2SiO_4 ringwoodite at high pressures. *Journal of Geophysical Research: Solid Earth*, *109*(12), B12209. https://doi.org/10.1029/2004JB003094

Katsura, T., Yoneda, A., Yamazaki, D., Yoshino, T., & Ito, E. (2010). Adiabatic temperature profile in the mantle. *Physics of the Earth and Planetary Interiors*, *183*(1–2), 212–218. https://doi.org/10.1016/j.pepi.2010.07.001

Kawamoto, T., & Holloway, J. R. (1997). Melting temperature and partial melt chemistry of H_2O-saturated mantle peridotite to 11 gigapascals. *Science*, *276*, 240–243. https://doi.org/10.1126/science.276.5310.240

Mao, Z., Jacobsen, S. D., Jiang, F., Smyth, J. R., Holl, C. M., Frost, D. J., & Duffy, T. S. (2008). Single-crystal elasticity of wadsleyites, β-Mg_2SiO_4, containing 0.37–1.66 wt.% H_2O. *Earth and Planetary Science Letters*, *266*(1–2), 78–89. https://doi.org/10.1016/j.epsl.2007.10.045

Matsui, M., Parker, S. C., & Leslie, M. (2000). The MD simulation of the equation of state of MgO: Application as a pressure calibration standard at high temperature and high pressure. *American Mineralogist*, *85*(2), 312–316. https://doi.org/10.2138/am-2000-2-308

Nishihara, Y., Doi, S., Kakizawa, S., Higo, Y., & Tange, Y. (2020). Effect of pressure on temperature measurements using WRe thermocouple and its geophysical impact. *Physics of the Earth and Planetary Interiors*, *298*, 106348. https://doi.org/10.1016/j.pepi.2019.106348

Pearson, D. G., Brenker, F. E., Nestola, F., McNeill, J., Nasdala, L., Hutchison, M. T., et al. (2014). Hydrous mantle transition zone indicated by ringwoodite included within diamond. *Nature*, *507*, 221–224. https://doi.org/10.1038/nature13080

Rudolph, M. L., Lekic, V., & Lithgow-Bertelloni, C. (2015). Viscosity jump in Earth's mid-mantle. *Science*, *350*, 1349–1352. https://doi.org/10.1126/science.aad1929

Sarafian, E., Gaetani, G. A., Hauri, E. H., & Sarafian, A. R. (2017). Experimental constraints on the damp peridotite solidus and oceanic mantle potential temperature. *Science*, *355*(6328), 942–944. https://doi.org/10.1126/science.aaj2165

Saxena, S. K., Chtterjee, N., Fei, Y., & Shen, G. (1993). *Thermodynamic data on oxides and silicates: An assessed data set based on thermochemistry and high pressure phase equilibrium*.(pp. 428) Springer-Verlag. https://doi.org/10.1007/978-3-642-78332-6

Sinogeikin, S. V., Bass, J. D., & Katsura, T. (2003). Single-crystal elasticity of ringwoodite to high pressures and high temperatures: Implications for 520 km seismic discontinuity. *Physics of the Earth and Planetary Interiors*, *136*, 41–66. https://doi.org/10.1016/S0031-9201(03)00022-0

Stixrude, L. (1997). Structure and sharpness of phase transitions and mantle discontinuities. *Journal of Geophysical Research: Solid Earth*, *102*(7), 14835–14852. https://doi.org/10.1029/97JB00550

Tange, Y., Kuwayama, Y., Irifune, T., Funakoshi, K., & Ohishi, Y. (2012). *P-V-T* equation of state of $MgSiO_3$ perovskite based on the MgO pressure scale: A comprehensive reference for mineralogy of the lower mantle. *Journal of Geophysical Research: Solid Earth*, *117*(6), B06201. https://doi.org/10.1029/2011JB008988

Tange, Y., Nishihara, Y., & Tsuchiya, T. (2009). Unified analyses for *P-V-T* equation of state of MgO: A solution for pressure-scale problems in high *P-T* experiments. *Journal of Geophysical Research: Solid Earth*, *114*(3), B03208. https://doi.org/10.1029/2008JB005813

Turcotte, D. L., & Schubert, G. (2014). *Geodynamics* (3rd ed.). Cambridge University Press, pp.1475. https://doi.org/10.1017/CBO9780511843877

Waszek, L., Tauzin, B., Schmerr, N. C., Ballmer, M., & Alfonso, J. C. (2021). A poorly mixed mantle transition zone and its thermal state inferred from seismic waves. *Nature Geoscience*, *14*, 949–955. https://doi.org/10.1038/s41561-021-00850-w

Watanabe, H. (1982). Thermochemical properties of synthetic high-pressure compounds relevant to the Earth's mantle. In S. Akimoto, & M. H. Manghnani (Eds.), *High-pressure research in geophysics* (pp. 441–464). Center for Academic Publications. https://link.springer.com/gp/book/9789027714398

Wolf, A. S., Jackson, J. M., Dera, P., & Prakapenka, V. B. (2015). The thermal equation of state of (Mg, Fe)SiO_3 bridgmanite (perovskite) and implications for lower mantle structures. *Journal of Geophysical Research: Solid Earth*, *120*(11), 7460–7489. https://doi.org/10.1002/2015JB012108

Xu, W.B., Lithgow-Bertelloni, C., Stixrude, L., & Ritsema, J., (2008). The effect of bulk composition and temperature on mantle seismic structure. *Earth and Planetary Science Letters*, *275*(1–2), 70–79. https://doi.org/10.1016/j.epsl.2008.08.012

Yagi, T., Akaogi, M., Shimomura, O., Suzuki, T., & Akimoto, S.-I. (1987). In situ observation of the olivine-spinel phase transformation in Fe_2SiO_4 using synchrotron radiation. *Journal of Geophysical Research: Solid Earth*, *92*(7), 6207–6213. https://doi.org/10.1029/JB092iB07p06207